

Adaptive tracking of EEG oscillations

Jérôme Van Zaen^{a,*}, Laurent Uldry^a, Cédric Duchêne^a, Yann Prudat^a, Reto A. Meuli^{b,d},
Micah M. Murray^{b,c,d}, Jean-Marc Vesin^a

^a Signal Processing Laboratory, Swiss Federal Institute of Technology, Lausanne, Switzerland

^b Center for Biomedical Imaging of Lausanne and Geneva, Switzerland

^c Neuropsychology and Neurorehabilitation Service, Centre Hospitalier Universitaire Vaudois and University of Lausanne, Switzerland

^d Radiology Service, Centre Hospitalier Universitaire Vaudois and University of Lausanne, Switzerland

ARTICLE INFO

Article history:

Received 1 July 2009

Received in revised form 9 October 2009

Accepted 23 October 2009

Keywords:

Adaptive tracking

Neuronal oscillations

Cross-frequency couplings

EEG

ABSTRACT

Neuronal oscillations are an important aspect of EEG recordings. These oscillations are supposed to be involved in several cognitive mechanisms. For instance, oscillatory activity is considered a key component for the top-down control of perception. However, measuring this activity and its influence requires precise extraction of frequency components. This processing is not straightforward. Particularly, difficulties with extracting oscillations arise due to their time-varying characteristics. Moreover, when phase information is needed, it is of the utmost importance to extract narrow-band signals. This paper presents a novel method using adaptive filters for tracking and extracting these time-varying oscillations. This scheme is designed to maximize the oscillatory behavior at the output of the adaptive filter. It is then capable of tracking an oscillation and describing its temporal evolution even during low amplitude time segments. Moreover, this method can be extended in order to track several oscillations simultaneously and to use multiple signals. These two extensions are particularly relevant in the framework of EEG data processing, where oscillations are active at the same time in different frequency bands and signals are recorded with multiple sensors. The presented tracking scheme is first tested with synthetic signals in order to highlight its capabilities. Then it is applied to data recorded during a visual shape discrimination experiment for assessing its usefulness during EEG processing and in detecting functionally relevant changes. This method is an interesting additional processing step for providing alternative information compared to classical time–frequency analyses and for improving the detection and analysis of cross-frequency couplings.

© 2009 Elsevier B.V. All rights reserved.

1. Introduction

Oscillatory phenomena have been the focus of increasing interest in neuroscience research. Neuronal oscillations have been proposed as a key mechanism for the large-scale integration of cognitive processes through which top-down internal states influence stimulus processing (Engel et al., 2001; Varela et al., 2001). Several models have been developed, with oscillations either serving as a binding mechanism bringing together different perceptions into a unified representation (Singer and Gray, 1995; Engel and Singer, 2001) or as a dynamic substrate for neuronal communication achieved through the coherence between brain areas (Fries, 2005). Also a more precise observation of specific oscillatory parameters can shed light on even more detailed brain processes. For instance, the ongoing oscillatory state of the brain before a given stimulus has been shown to provide valuable information

about the subsequent behavioral responses in both motor and sensory tasks (Linkenkaer-Hansen et al., 2004; Womelsdorf et al., 2006). Additionally, the phase of neuronal oscillations was successfully linked to activity of single neurons (Jacobs et al., 2007). Finally, increasing evidence indicates that responses within classical neuronal frequency bands likely interact with each other through coupling mechanisms that remain to be identified (Jensen and Colgin, 2007). In this framework, cross-frequency couplings could provide a unifying mechanism for the intermingled neuronal oscillations acting at different temporal and spatial scales (Von Stein and Sarnthein, 2000), and recent studies tend to verify the existence, and the possible importance of cross-frequency couplings, during a variety of motor, sensory and cognitive tasks (Canolty et al., 2006; Lakatos et al., 2007; Demiralp et al., 2007).

Taken together, these findings raise the need for efficient methods for accurate estimation of oscillatory information such as phase, frequency and amplitude from raw signals. A well-known method widely used to get such spectral information is the Hilbert transform and its analytic signal representation (Gabor, 1946). However,

* Corresponding author. Tel.: +41 21 693 56 51; fax: +41 21 693 76 00.
E-mail address: jerome.vanzaen@epfl.ch (J. Van Zaen).

although many studies have successfully identified and described phase synchronizations by applying this method to wide-band neuronal signals, it has been shown that proper estimation of oscillatory parameters can be performed only on narrow-band signals (Nho and Loughlin, 1999; Chavez et al., 2006). Moreover, subsequent synchronization measures such as the Phase Locking Value (Tass et al., 1998) are reliable only when applied to narrow-band signals (Celka, 2007). Therefore, band-pass filtering was applied to neuronal signals as a pre-processing step, in order to split the raw signals into narrow-band oscillations of different frequencies. Although this filter bank approach can lead to a more reliable analysis of oscillatory interactions (Canolty et al., 2006), a major drawback of such pre-processing should be mentioned. Because the cut-off frequencies of each band-pass filter must be pre-defined and remain constant during the whole analysis window, physiologically misleading outputs could be produced by the filters, in the case of a frequency component crossing the cut-off frequency limit of a filter. In such situations, it would be preferable to follow an oscillatory component in a continuous manner, without constraining the spectral content to fixed limits. This remark emphasizes the need for adaptive methods able to track narrow-band oscillations over time.

Recently, we proposed a novel method for adaptively tracking multiple oscillations in single-trial EEG signals (Uldry et al., 2009). In this article, we describe the tracking abilities of our algorithm for the estimation of single or multiple frequencies in both synthetic and EEG signals. The physiological relevance of well-known synchronization measures can be assessed using the temporal outputs of our method. Importantly, our previous publication on this tracking scheme is extended in order to clearly illustrate its capabilities for adaptive frequency estimation and its advantages over more traditional approaches for measuring cross-frequency couplings. In Section 2, we present the basics of our algorithm as well as its multi-frequency and multi-signal extensions, and we illustrate its performance on synthetic signals. In Section 3, we present the results of our method on real EEG single-trial signals in terms of adaptive frequency tracking, and demonstrate the benefit of applying common synchronization measures on the temporal outputs of our filters, compared to current methods.

2. Methods

The oscillation tracking methods are presented within the complex-valued signal framework. This approach simplifies several aspects of the computations. Especially, the filters are shorter (only one pole is needed for a complex band-pass filter, whereas two poles are required for a real band-pass filter). Of course, the signals of interest are real-valued in practice. But with the Hilbert transform one obtains the so-called analytic representation, whose real part is the original signal itself. Therefore, it is always possible to revert back to real-valued signals.

2.1. Frequency tracking

The frequency tracking algorithm presented in this paper is based on a real-valued scheme (Liao, 2005). It is composed of two parts; a time-varying band-pass filter and an adaptive mechanism that controls the central frequency of the filter. The structure is shown in Fig. 1. The input signal is defined as

$$x(n) = d(n) + w(n) = A(n)e^{j\omega(n)n} + w(n),$$

where $A(n)$ and $\omega(n)$ are the amplitude and the instantaneous frequency of the cisoid and $w(n)$ is an additive white complex centered noise. The output signal, $y(n)$, is obtained by filtering the input

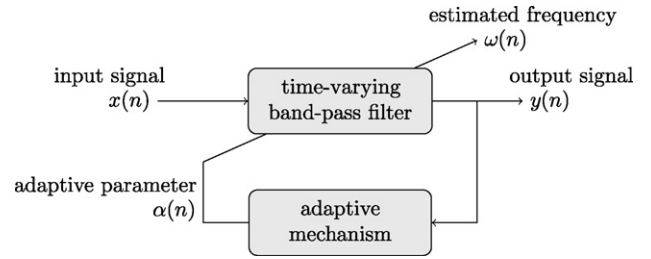


Fig. 1. Frequency tracking algorithm structure.

signal with a band-pass filter, with transfer function

$$H(z, n) = \frac{1 - \beta}{1 - \beta\alpha(n)z^{-1}}. \quad (1)$$

The bandwidth is determined by β ($0 \ll \beta < 1$) and $\alpha(n) = e^{j\omega(n)}$ is the adaptive parameter which controls the central frequency. This filter has unit gain and zero phase at $\omega(n)$.

The mechanism, which tracks the oscillations and updates the filter, is based on the complex discrete oscillator equation

$$d(n) = e^{j\omega_0}d(n-1) = \alpha_0d(n-1). \quad (2)$$

This equation is satisfied for a cisoid at frequency ω_0 . Therefore given $d(n)$ and $d(n-1)$, it is possible to obtain the frequency with

$$\omega_0 = \text{Arg}\{\alpha_0\}, \quad \alpha_0 = \frac{d(n)}{d(n-1)}.$$

In a time-varying and noisy scenario, the coefficient $\alpha(n+1)$ can be estimated by minimizing the mean square error (MSE) of the oscillator equation (2) for the output signal, $y(n)$, of the adaptive filter (1):

$$J(n) = E\{|y(n) - \alpha(n+1)y(n-1)|^2\}. \quad (3)$$

Setting $\partial J(n)/\partial \alpha(n+1) = 0$, the optimal solution is

$$\alpha(n+1) = \frac{E\{y(n)\bar{y}(n-1)\}}{E\{|y(n-1)|^2\}}$$

where the upper bar denotes the complex conjugate. However, this expression is not applicable in practice. Therefore, the expectations are replaced by exponentially weighted averages (Haykin, 2001), and the adaptive mechanism becomes

$$\alpha(n+1) = \frac{Q(n)}{P(n)} = \frac{\delta Q(n-1) + [1 - \delta]y(n)\bar{y}(n-1)}{\delta P(n-1) + [1 - \delta]|y(n-1)|^2} \quad (4)$$

where δ ($0 \ll \delta < 1$) controls the convergence rate. The modulus of coefficient $\alpha(n+1)$ is then brought back to unity to ensure the stability of the band-pass filter. Finally, the frequency estimate is obtained with $\omega(n+1) = \text{Arg}\{\alpha(n+1)\}$.

2.2. Multiple frequency tracking

Typically, multiple oscillatory components are active at the same time in EEG signals. The method described previously can be extended to the multi-component case. Now, it is assumed that the input signal is composed of K cisoids with additive complex noise, i.e.

$$x(n) = \sum_{k=1}^K d_k(n) + w(n) = \sum_{k=1}^K A_k(n)e^{j\omega_k(n)n} + w(n)$$

where $A_k(n)$ and $\omega_k(n)$ are the amplitude and the instantaneous frequency of the k th cisoid and $w(n)$ is an additive white complex centered noise. The basic idea of the extension is to use one frequency tracking algorithm from Section 2.1 to track each component. However, because the band-pass filters (1) are not ideal

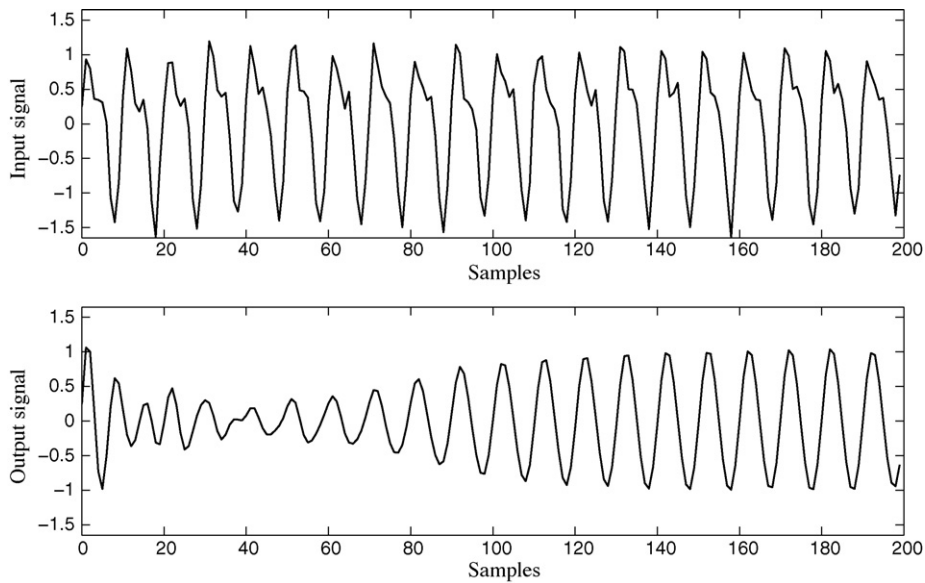


Fig. 2. Frequency tracking example. (top) Input signal; (bottom) output signal of the single frequency tracking scheme.

ones, each of them will “see” the other components. This can lead to errors, especially for components close in the frequency domain. A solution to this problem is to use all-zero filters to cancel interference from other components (Rao and Kumarasan, 2000).

The number of components K is assumed to be known. Each component is tracked with two adaptive filters; an all-zero filter and a band-pass filter. The band-pass filter is the same as for the single frequency case (1). The all-zero filter is composed of $p - 1$ complex zeros whose locations are defined by the frequencies $\{\omega_i(n)\}_{i=1, i \neq k}^p$. The transfer function of the k th all-zero filter is

$$G_k(z, n) = C_k(n) \prod_{\substack{i=1 \\ i \neq k}}^K [1 - \gamma e^{j\omega_i(n)} z^{-1}]$$

where γ ($0 \ll \gamma \leq 1$) is the modulus of the zero and $C_k(n)$ is a normalization coefficient to ensure unit gain and zero phase at frequency $\omega_k(n)$. Because the true frequencies are unknown, they are replaced with their estimates in the filters.

However, the additional all-zero filters introduce perturbation in the global response, which might not be pure band-pass anymore, resulting in unwanted frequencies leaking to the output. Moreover, longer filters reduce the convergence rate of the algorithm. An alternative is to select only one zero for the k th all-zero filter. This zero is placed at the tracked frequency closest to the k th frequency. This solution offers a good tradeoff between interference suppression, tracking speed and the band-pass characteristic of the overall filter.

2.3. Multi-signal extension

In several practical situations, particularly with EEG/MEG signals, the information of interest is observed with multiple sensors. These signals are often highly correlated. Therefore, instead of tracking the frequencies separately for each signal, the joint processing will improve the tracking performance, the convergence speed and the robustness of the adaptive algorithm (Prudat and Vesin, 2009). This joint processing is done by applying the same filters to each signal. These filters are then updated jointly with a weighted update. The weights are chosen in order to favor the signals that better satisfy the oscillation cost function (3). Therefore,

the weights are obtained by dividing an estimate of the band-pass filter output variance by an estimate of (3). The output variance is used to yield a scale-independent scheme.

In practice, the cost function and output variance estimates are computed with exponentially weighted averages. The cost function instantaneous estimate $\hat{J}_{k,m}(n)$ for the k th band-pass filter for the m th signal is defined as

$$\hat{J}_{k,m}(n) = \delta \hat{J}_{k,m}(n-1) + [1 - \delta] |y_{k,m}(n) - \alpha_k(n) y_{k,m}(n-1)|^2$$

where δ is the same forgetting factor as the one used in (4), and $y_{k,m}(n)$ is the output of the k th band-pass filter for the m th signal. Analogously, the output variance instantaneous estimate $\hat{S}_{k,m}(n)$ of the k th band-pass filter for the m th signal is given by:

$$\hat{S}_{k,m}(n) = \delta \hat{S}_{k,m}(n-1) + [1 - \delta] |y_{k,m}(n)|^2.$$

The weights are then:

$$W_{k,m}(n) = \frac{\hat{S}_{k,m}(n) / \hat{J}_{k,m}(n)}{\sum_{l=1}^M \hat{S}_{k,l}(n) / \hat{J}_{k,l}(n)}.$$

Finally, the update of the k th tracked frequency is:

$$\omega_k(n+1) = \sum_{m=1}^M W_{k,m}(n) \omega_{k,m}(n+1)$$

where $\omega_{k,m}(n+1)$ is the k th frequency tracked separately for the m th signal. The update is performed on the tracked frequencies instead of directly updating the adaptive coefficients $\alpha_k(n+1)$ as was done in (4). This modification is made necessary because a weighted update of the unit-modulus $\alpha_{k,m}(n+1)$ will not lead to a unit-modulus $\alpha_k(n+1)$.

2.4. Examples on synthetic signals

The capabilities of these frequency tracking algorithms are illustrated with a few synthetic signals. The first example illustrates the interpretation problem of the instantaneous phase (obtained with the Hilbert transform) when the signal is not narrow-band. A simple signal composed of two sinusoids with additive white Gaussian

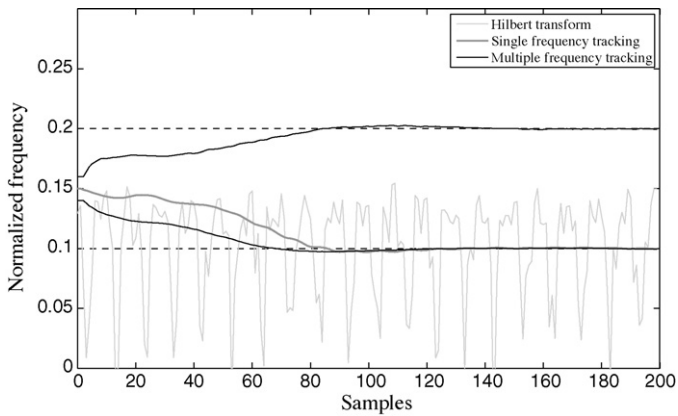


Fig. 3. Frequency tracking example. The dashed black lines denote the true frequencies.

noise (AWGN) is considered. It is defined as

$$x(n) = \sin(2\pi 0.1n) + \frac{1}{2} \sin\left(2\pi 0.2n + \frac{\pi}{4}\right) + w(n) \quad (5)$$

where $w(n)$ is the AWGN with variance set to 0.01 (SNR of 17 dB for the first sinusoid and 11 dB for the second sinusoid). The frequencies are estimated with the Hilbert transform (differentiation of the phase), the single frequency tracker and the multiple frequency tracker (set to track two components). The parameters of the adaptive schemes are set as follows, $\beta = 0.95$, $\delta = 0.95$, $\gamma = 1$. The initial frequencies are 0.15 for the single frequency tracker and 0.14 and 0.16 for the multiple frequency tracker.

The input signal (5) is shown, along with the output from the single frequency tracker, in Fig. 2, while the frequency estimates are shown in Fig. 3. Intuitively, the instantaneous frequency should be located between the true frequencies (0.1 and 0.2), which is not the case in this example due to the broad-band characteristic of the signal. In fact, even without AWGN, the instantaneous frequency estimate obtained with the Hilbert transform is still approximately the same (not shown). However, these results can be improved by smoothing the instantaneous frequency at the cost of temporal resolution, because the smoothing filter should be rather long. Nevertheless, both adaptive schemes provide sensible results after approximately 100 samples. The single frequency tracker selects only one component, depending on its power and the initialization. The multiple frequency tracker converges slightly earlier due to the all-zero filters which attenuate the cross-frequency interferences. Moreover, the output signals of the trackers (the output of the single frequency tracker is shown in Fig. 2) are narrow-band signals and their phase can be extracted with the Hilbert transform for further processing without interpretation problems.

Next, a multiple frequency tracking example is presented. The signal is composed of three oscillatory components and AWGN. The SNR is set to 10 dB with respect to each component. The first component is a sinusoid with a shift in frequency from 0.1 to 0.2 after 400 samples, the second one is a chirp from 0.2 to 0.45, and the third one is a chirp from 0.45 to 0.1. The multiple frequency tracker is applied with the following parameters and initial frequencies: $\beta = 0.975$, $\delta = 0.95$, $\gamma = 0.95$, $f_1(0) = 0.1$, $f_2(0) = 0.2$ and $f_3(0) = 0.45$. The results are shown in Fig. 4. One observes that the frequency estimates follow closely the true frequencies (denoted by dashed lines) and that they even can cross each other to track the time-varying frequencies.

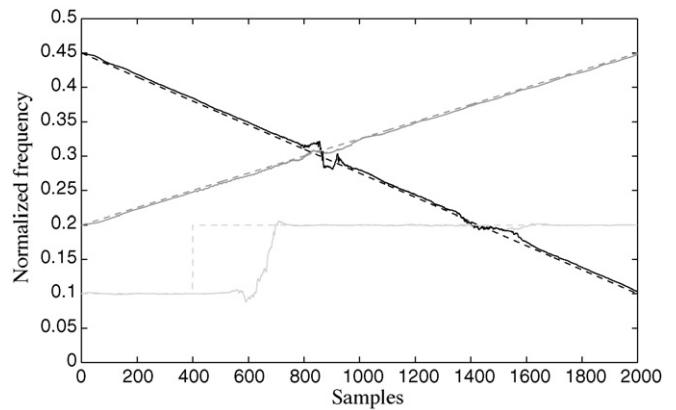


Fig. 4. Multiple frequency tracking example. The dashed lines denote the true frequencies.

3. Results

The data we present have been taken from a previously published study examining the spatio-temporal mechanisms of illusory contour perception with broad-band event-related potentials (Murray et al., 2002). This paradigm was chosen here as it represents a typical situation where time–frequency analyses based on wavelet decomposition have been extensively applied and have led to propositions regarding the role of gamma oscillations as a binding mechanism in human cortex (Tallon-Baudry and Bertrand, 1999). Full paradigmatic details can be obtained in the original study. Here, we provide only the most relevant details.

Participants in the study viewed arrays of ‘pac-man’ inducers that were presented in either of two orientations. In the illusory contour (IC) condition, the ‘mouths’ of the inducers were oriented so as to produce the illusory perception of a central square. In the no contour (NC) condition, the inducers were all turned 180° outwards to prevent the perception of a central illusory square (see Fig. 5 for an example). The timing of presentations was such that each stimulus appeared for 500 ms, followed by a blank screen for 1000 ms. Then a Y/N response prompt appeared and remained on the screen until a response was made, allowing subjects to control stimulus delivery. A blank screen (1000 ms duration) followed responses. Use of the response prompt was motivated by the desire to diminish the impact of motor responses on the sensory event-related potentials.

Continuous EEG was acquired through Neuroscan Synamps from 64 scalp electrodes (impedances $\leq 5 \text{ k}\Omega$), referenced to the nose, band-pass filtered from 0.05 to 100 Hz, and sampled at 500 Hz.

The EEG signals of two subjects were investigated. For the first subject (respectively the second subject) 279 trials (262 trials) for condition IC and 276 trials (265 trials) for condition NC were visually selected with the Cartool software by Denis Brunet (<http://brainmapping.unige.ch/Cartool.htm>). A threshold of $\pm 80 \mu\text{V}$ for artifact rejection was used for each epoch. Each trial represents 2000 ms of EEG data, with the stimulus onset at 500 ms.

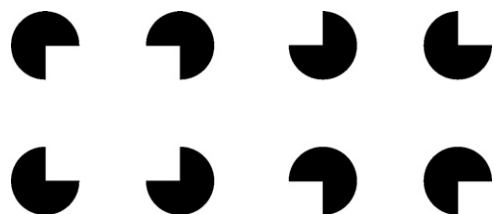


Fig. 5. Example of visual stimuli: illusory contour (IC, left) and no contour (NC, right).

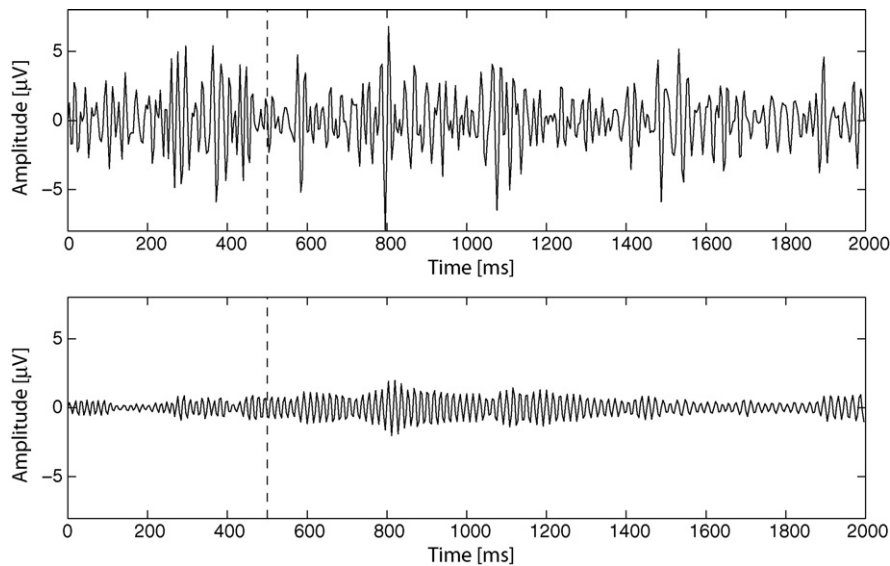


Fig. 6. Frequency tracking on an EEG signal for the IC condition: input signal (top) and output signal (bottom).

Once the trials were extracted, all further processing was performed in Matlab®.

The parieto-occipital electrode PO4 was selected as it is the one where the maximal difference was obtained in the broad-band event-related potential (see Murray et al. (2002) for details). This signal was processed as follows. It was resampled at 250 Hz and filtered into two bands: θ -band (4–8 Hz) and γ -band (30–80 Hz). Finally, the single frequency tracking algorithm was applied to these two bands in order to obtain the filtered outputs and the frequency estimates. The algorithm was initialized with the mirrored first 500 ms of each trial, the frequency estimates were initialized to the central frequency of each band (6 Hz for θ -band and 55 Hz for γ -band) and the parameters were set to $\beta = 0.975$ and $\delta = 0.95$. This choice of parameters results from a tradeoff between tracking speed and estimation variance. Practically, the tracking scheme was applied to a subset of EEG data for various parameter values. The frequency estimates and filtered outputs were then visually inspected in order to select the parameters that yield the best compromise between convergence speed and tracking accuracy. The procedure for initializing the tracked frequencies is rather rudimentary: the central frequency of each band is selected (or evenly spaced frequencies over the gamma band for the multi-frequency extension). Clearly, more sophisticated methods should be investigated, but, for the purpose of illustrating the tracking capabilities of the presented scheme, this basic initialization is sufficient.

An example of oscillation tracking for the γ -band is shown in Figs. 6 and 7. Fig. 6 shows the input signal in the top panel and the output signal in the bottom panel. The output signal contains only the oscillation tracked. Therefore, the tracker provides a narrow-band output signal compared to the broad-band input signal. In Fig. 7, frequency estimates are compared to a smoothed pseudo Wigner–Ville distribution (Flandrin, 1999) of the input signal. This type of time–frequency representation leads to a slightly better resolution for short-duration signals compared to short-time Fourier transform. It is computed with the Time Frequency Toolbox (<http://tftb.nongnu.org/>). The adaptive algorithm is able to track a given oscillation even if its frequency and amplitude vary over time. The sharp transition in the first 50 ms is due to the initialization of the internal variables ($Q(n)$ and $P(n)$) of the adaptive algorithm which increases its variability for a short duration. In order to alleviate this kind of problem, a narrower frequency band can be used or the multi-frequency tracker can be applied. Nonetheless, the

impact of the initialization process is very limited when applying the tracking scheme to a time segment larger than the period of interest. A burst of oscillatory activity at 40 Hz and 1500 ms seems to be ignored by the tracker. In fact, it is so because the tracker is already following another frequency component and the burst is not powerful enough to attract it.

Another example to illustrate the multiple frequency tracker, for the single-signal case and the multi-signal case, is shown in Fig. 8. The parameters are the same as for the single frequency case. All zeros are used for the zero filters and the modulus of the zeros is set to $\gamma = 1$. The initial frequencies are 42.5, 55 and 67.5 Hz. The estimated frequencies are compared with the smoothed pseudo Wigner–Ville distribution of the input signal. The results obtained with one electrode (PO4) and a cluster of electrodes (PO4, P4, PO6 and P6) are very similar. However, the multi-signal extension seems to track the oscillations more accurately by taking advantage of the redundant information of closely spaced electrodes. The gain in estimation accuracy when using more than one signal is difficult to assess with EEG data whose frequency components are not known a priori. However, with synthetic signals, the single-signal scheme can be compared rigorously to its multi-signal extension with Monte Carlo simulations; the gain in estimation

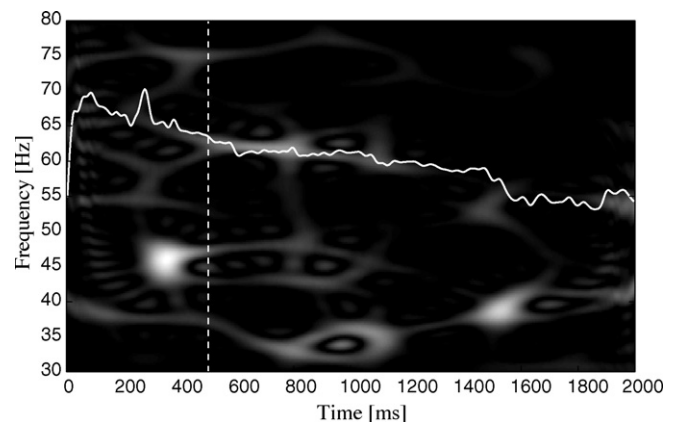


Fig. 7. Frequency tracking on an EEG signal for the IC condition: the estimated frequencies (white) follow closely a time-varying oscillation. The vertical white dashed line denotes stimulus onset.

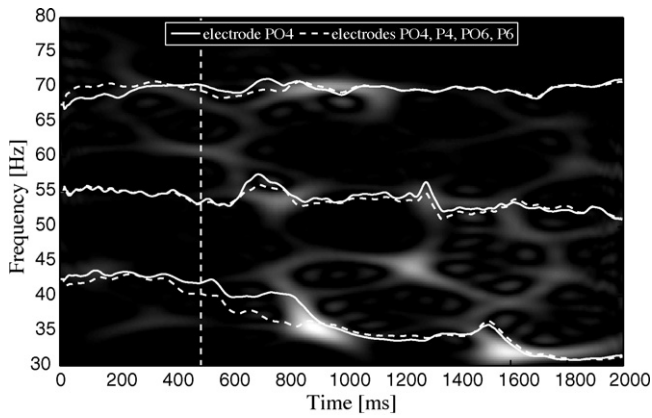


Fig. 8. Example of multiple frequency tracking on EEG signals for the IC condition: tracking on signal recorded with electrode PO4 (solid), tracking on signals recorded with electrodes PO4, P4, PO6 and P6 (dashed) and stimulus onset (vertical dashed).

variance is approximately M for M input signals (Prudat and Vesin, 2009).

3.1. Statistics

Two statistics for discriminating the IC and NC conditions were investigated. The first statistic is simply the mean estimated frequency in the θ -band, and the second statistic is the phase–phase coupling between the θ -band and the γ -band obtained with a synchronization measure. These statistics were estimated over sliding windows of lengths ranging from 100 ms to 1000 ms in 100 ms steps (tradeoff between time resolution and estimation precision), with time shift of 10 ms. The time shift was used to inspect the variations of the statistics over time. Then these estimates were transformed into approximately normal random variables, if needed, and two-sample t -tests with unequal variance were applied to compare conditions. Thus, the use of sliding windows provides time-varying p -values.

3.1.1. Mean estimated frequency

The tracking algorithm yields an instantaneous frequency estimate, which can be used to define a basic statistic. The mean

estimated frequency statistic is computed by averaging the frequency estimates of the tracker over a sliding window. Before comparing the two conditions with t -tests, a Jarque–Bera test (Jarque and Bera, 1987) was applied to ensure that this statistic follows approximately a normal distribution. The results of the comparison of the two conditions are shown in Fig. 9. It appears that the mean estimated frequency is significantly higher for IC than NC condition over the intervals 200–1000 ms for subject 1 and 300–800 ms for subject 2 with respect to stimulus onset. Moreover the p -values are very small in these intervals. For example, at $t = 1000$ ms, the p -value is smaller than 10^{-7} for subject 1 and 10^{-3} for subject 2.

3.1.2. Phase–phase couplings

The phase–phase couplings between the θ -band and the γ -band were measured with the phase synchronization index (PSI) (Mormann et al., 2000; Quiñero et al., 2002) (for similar approaches, see Tass et al., 1998; Lachaux et al., 1999). It is computed with the phases of the signals of interest.

The phase $\phi_x(n)$ of a signal $x(n)$ is extracted from the analytic signal, $Z_x(n) = x(n) + j\tilde{x}(n) = A_x(n)e^{j\phi_x(n)}$, where $\tilde{x}(n)$ is the discrete Hilbert transform of $x(n)$. The phase $\phi_y(n)$ of $y(n)$ is defined similarly. As mentioned previously, the physical interpretation of the phase of broad-band signals can be difficult (Nho and Loughlin, 1999; Celka, 2007). The signals $x(n)$ and $y(n)$ are said to be $a : b$ synchronized if their (a, b) phase difference, $a\phi_x(n) - b\phi_y(n)$, remains bounded for all n , with a and b positive integers. The PSI is defined as follows:

$$P_{x,y} = |E\{e^{j[a\phi_x(n) - b\phi_y(n)]}\}|. \quad (6)$$

It will be equal to one when the phase difference is constant (signals perfectly synchronized) and will be equal to zero when the signals are not synchronized at all. In practice, the expectation in (6) is replaced with the sample mean.

The PSI is computed with the phase of the θ -oscillation, $\phi_\theta(n)$ and the phase of the γ -oscillation, $\phi_\gamma(n)$, and for coefficients (a, b) values $(6, 1)$, $(7, 1)$ and $(8, 1)$. Additionally, in order to compare the classical approach and the adaptive tracking approach, the phases are extracted from the signals filtered with the fixed band-pass filters and from the output signals of the frequency tracking algorithm. Then the PSIs are transformed into approximately normal

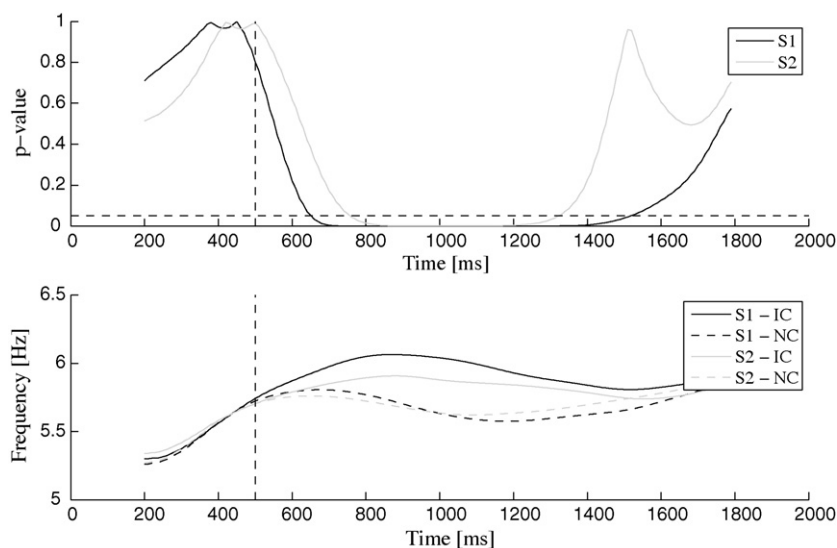


Fig. 9. Mean estimated frequency computed over a 400 ms window. (top) p -value for the difference between IC and NC for each subject and (bottom) mean estimated frequency over trials for each subject and each condition. The vertical dashed lines indicate stimulus onset and the horizontal dashed line is the 5% significance level.

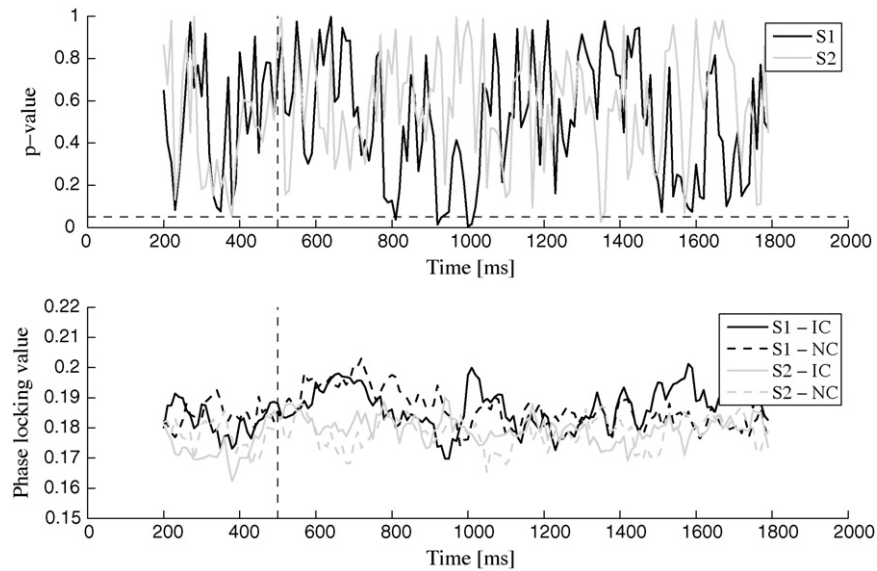


Fig. 10. Phase–phase couplings computed with the outputs of the fixed band-pass filters between the θ -band and the γ -band over a 400 ms window, $(a, b) = (7, 1)$. (top) p -value for the difference between IC and NC for each subject and (bottom) mean PSI over trials for each subject and each condition. The vertical dashed lines indicate stimulus onset and the horizontal dashed line is the 5% significance level.

random variables with an arcsine transform (Penny et al., 2008):

$$Z_{x,y} = \arcsin(2P_{x,y} - 1).$$

Finally, a two-sample t -test with unequal variance is applied to compare the IC and NC conditions for each subject.

The results obtained without the frequency tracking algorithm for $(a, b) = (7, 1)$ are shown in Fig. 10. Clearly, no significant difference between IC and NC for either of the subjects is observed.

Applying the frequency tracking scheme before computing the PSIs leads to better results, as shown in Fig. 11. The PSI, computed with $(a, b) = (7, 1)$, is significantly higher for condition IC in the interval 330–430 ms with respect to stimulus onset for both subjects. In this interval, the p -value reaches values as low as 10^{-3} for subject 1 and 10^{-4} for subject 2.

The results obtained with the frequency tracking algorithm, with (a, b) set to $(6, 1)$ and $(8, 1)$, are shown in Figs. 12 and 13

respectively. In both cases, there are significant differences (higher PSIs for IC) between conditions IC and NC in similar intervals as for $(a, b) = (7, 1)$. However, from these observations, the choice of the coupling coefficients (a, b) that yields the most significant differences seems to be subject-dependent. For subject 1, the choice $(a, b) = (6, 1)$ appears to be the most appropriate, while for subject 2 it is $(a, b) = (7, 1)$. The results obtained without the adaptive scheme are not presented for the coupling coefficients $(6, 1)$ and $(8, 1)$ because they are very similar to the case $(a, b) = (7, 1)$ and show no significant difference.

4. Discussion

Oscillatory phenomena have gained increasing importance in the field of neuroscience, particularly because improvements in analysis methods have revealed how oscillatory activity is both

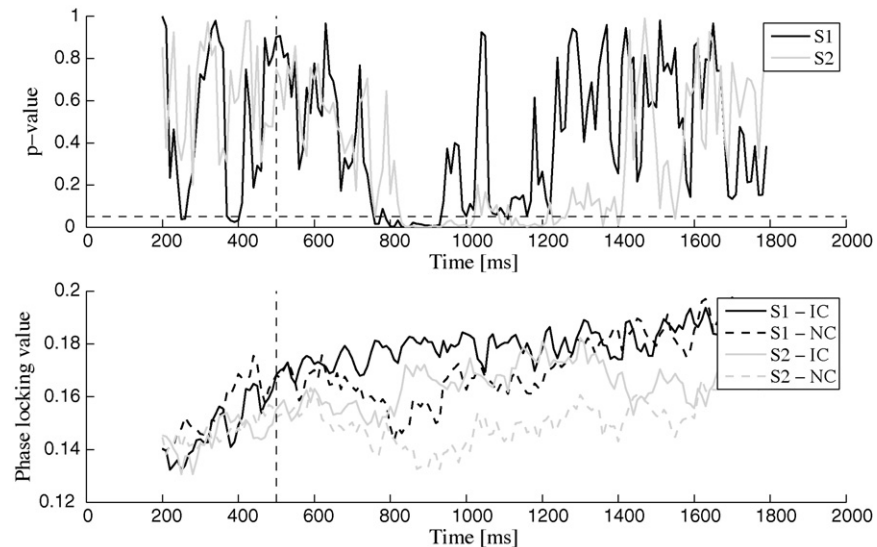


Fig. 11. Phase–phase couplings between the θ -band and the γ -band over a 400 ms window computed with the outputs of the frequency tracking algorithm, $(a, b) = (7, 1)$. (top) p -value for the difference between IC and NC for each subject and (bottom) mean PSI over trials for each subject and each condition. The vertical dashed lines indicate stimulus onset and the horizontal dashed line is the 5% significance level.

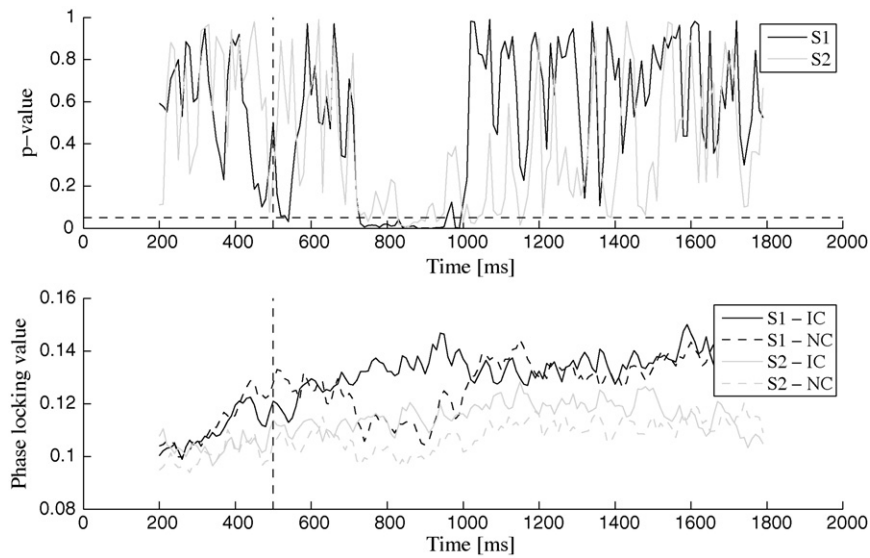


Fig. 12. Phase–phase couplings between the θ -band and the γ -band over a 400 ms window computed with the outputs of the frequency tracking algorithm, $(a, b) = (6, 1)$. (top) p -value for the difference between IC and NC for each subject and (bottom) mean PSI over trials for each subject and each condition. The vertical dashed lines indicate stimulus onset and the horizontal dashed line is the 5% significance level.

a highly efficient and also information-rich signal. One paradigmatic shift in the conceptualization of oscillatory activity has been to consider not only changes within a particular frequency band, but also the interactions and synchronizations between frequencies of brain activity that are in turn thought to coordinate responses between widespread brain areas and may represent a key “binding” mechanism necessary for perception, consciousness and actions. The methods developed here focus on the non-invasive and quantitative assessment of such oscillatory activity. In particular, the adaptive tracking scheme developed here can precisely extract a time-varying oscillation as well as estimate its frequency. It combines, to a certain extent, the advantages of narrow and wide band-pass filters while avoiding many of their drawbacks. Moreover, extensions to multiple components and multiple signals are possible that take into account some important characteristics of EEG data: several oscillations are active simultaneously and redun-

dant information can be carried across sensors. In what follows we first discuss the implications of these methods from a signal analysis perspective. We then consider some potential applications of these methods to neuroscientific research.

The adaptive algorithm and its extensions described in this paper are specifically aimed at tracking oscillations. The updating mechanism is designed to minimize an oscillatory criterion (3). An important point is that it is not based on a signal model, but merely assumes that oscillatory activity is an important aspect of EEG data. With such a cost function, oscillations can be extracted even during low amplitude data segments. This provides additional information compared to traditional time–frequency analysis where, below a certain power level, an oscillation can no longer be observed. Moreover, the oscillations are extracted with an adaptive band-pass filter, which can be made extremely narrow (at the cost of tracking speed). This filter has unit gain and zero phase at its central

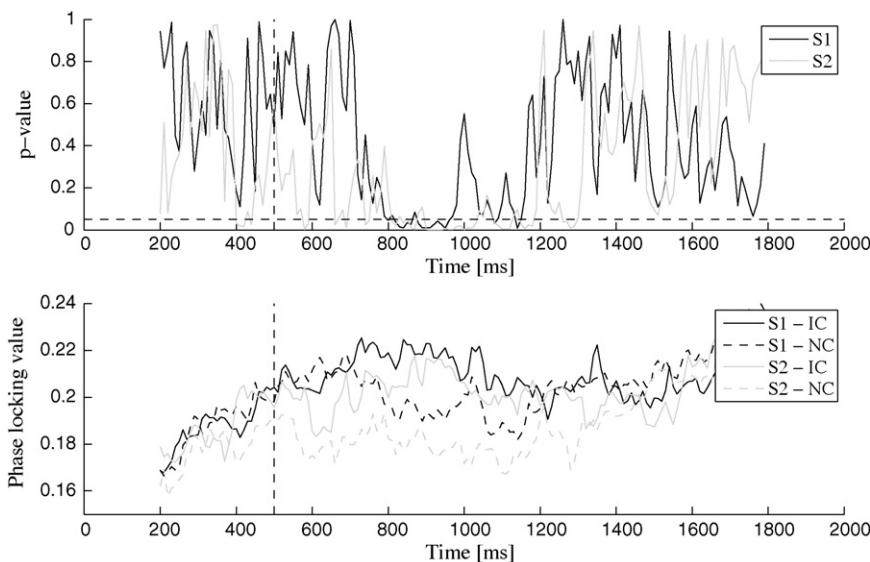


Fig. 13. Phase–phase couplings between the θ -band and the γ -band over a 400 ms window computed with the outputs of the frequency tracking algorithm, $(a, b) = (8, 1)$. (top) p -value for the difference between IC and NC for each subject and (bottom) mean PSI over trials for each subject and each condition. The vertical dashed lines indicate stimulus onset and the horizontal dashed line is the 5% significance level.

frequency, which is extremely important for further processing when phase extraction is involved. With these characteristics, this tracking method is a particularly appropriate tool for EEG (and MEG) data processing and analyses.

Traditional methods for extracting oscillations rely on fixed band-pass filtering. While this approach has proved to be useful, it has a few drawbacks. If a wide frequency band is chosen to take into account the time-varying frequency of the considered oscillation, noise and interfering oscillations will leak through the filter. Therefore, the output signal will not be narrow-band, and its instantaneous phase will be difficult to interpret. If, on the contrary, a narrow band-pass filter is selected, the phase of the output signal will be reliable. However, a time-varying oscillation will not be extracted over its whole duration, because its frequency will sometimes be outside of the chosen frequency band. The tracking scheme presented here is motivated by this tradeoff between respective benefits of a wide filter and a narrow filter. The filtering operation will damp the transients, but this problem is inherent to all methods based on filters. Nevertheless, when investigating coupling mechanisms, this adaptive scheme might still prove useful.

Some limitations of the present approach are also worth mentioning. Due to the adaptation process, it would be difficult to track an oscillatory component whose frequency varies very rapidly. But, in most cases for EEG signals, the changes in frequency are relatively smooth, letting the adaptive filter follow the considered oscillation precisely (maybe with a slight delay after abrupt changes). It can still track oscillatory components with shifting frequency as long as the shifts are not too large and not too frequent. Short-duration bursts of oscillatory activity might also be missed by the proposed method, especially bursts isolated in the frequency domain. Indeed, such bursts are too short to have a decisive impact on the tracker. Nevertheless, the tracking scheme can still be applied as a pre-processing tool when investigating cross-frequency couplings. Indeed, several studies measured such couplings on long time segments (Canolty et al., 2006) wherein extremely short oscillatory bursts have very limited impact. Another issue concerns the multi-component extension. By cascading several all-zero filters, the resulting filter loses its pure band-pass response. But this problem can be handled by picking only the closest zero, at the cost of slight interference leaking (as mentioned in Section 2.2). Another important aspect is that this oscillation tracking scheme still requires fixed band-pass filtering. Usually the power spectral density is inversely proportional to frequency ($1/f^\alpha$ spectrum) in EEG data (Freeman et al., 2000). Thus, the presented algorithm will not be able to extract a high-frequency oscillation if the high-amplitude low-frequency components have not been filtered out. Nevertheless, it is clearly possible to use wide band-pass filters before applying the tracking scheme, as was done in Section 3.1.2. An important aspect should still be emphasized for the single frequency tracker: it can only extract one frequency component and in a wide frequency band there is usually more than one active oscillation at a given time. Thus, some information might be lost. This problem is also present when using the multi-frequency extension but its impact is much less important. Indeed, the present method cannot detect the appearance or disappearance of oscillations. Therefore, when the multi-frequency extension is applied with three filters (for example), it is not able to handle a fourth component and simply ignores it. Nonetheless, we hope to improve the tracker in order to detect arising and fading components and adapt the number of filters.

The tracking capabilities of the presented adaptive algorithm were first evaluated with synthetic signals. An important aspect is its robustness for frequency estimation compared to the Hilbert transform for signals that are not strictly narrow-band. Moreover, several time-varying oscillations can be extracted simultaneously.

The oscillation tracking method was applied to EEG data in order to assess its usefulness for EEG processing. Two statistics revealed significant differences between experimental conditions (here the presence/absence of an illusory visual percept) recorded during a visual evoked potential experiment. The first statistic indicates that the frequency increase in the θ -band is significantly higher for the IC than for the NC condition. The second statistic shows a higher phase–phase coupling between the θ -band and the γ -band for IC than NC trials. An interesting point is that significant effects were only obtained with the oscillation tracking scheme. So it seems that the oscillation of interest is overshadowed by interference and noise when measuring phase–phase couplings over the whole band. An alternative, though in our view unlikely possibility, is that the present methods are overly prone to false positives.

The differences between experimental conditions were significant for the coefficients (6, 1), (7, 1) and (8, 1). This suggests that the γ -oscillation is 6–8 times faster than the θ -oscillation, or, alternatively, that during one θ -cycle, there are between 6 and 8 γ -cycles, depending on the individual. While further research is required to establish objective and quantitative methods for the selection of a particular coefficient, the present results nonetheless highlight how functionally relevant inter-individual variations in oscillatory brain activity can also be detected and discerned using the current approach. In addition, these methods can likely facilitate the evaluation of putative hierarchical relationships between oscillatory phenomena (Schroeder and Lakatos, 2009a,b). Still, a clear direction for continued development will be the application of these tracking procedures to estimated intracranial signals throughout the brain volume (Gonzalez Andino et al., 2005a,b; Martuzzi et al., 2009).

The development of the methods described in this manuscript has been driven by an increased understanding of the role of neuronal oscillations in sensory-cognitive information processing. There is now widespread consensus that sensory-cognitive processing is actively controlled by top-down influences, instead of treating external stimuli in a passive, purely bottom-up manner (Varela et al., 1991; Engel et al., 2001). Recent findings support the fundamental role of oscillatory activity in the top-down control of perception and brain responses (Buzsaki, 2006). Several hypotheses have been formulated in order to describe the role of oscillations and their relations with specific brain functions and behaviors. But, at this time, these relations remain poorly understood. Another aspect of the brain oscillatory activity is the interaction of oscillations in different frequency bands. These interactions take place through coupling mechanisms (Jensen and Colgin, 2007). Such cross-frequency couplings could be the mechanism by which oscillations in different frequency bands are unified. Cross-frequency couplings can manifest as interactions between amplitude, phase and frequency of the observed signal, including nested oscillations (Canolty et al., 2006) or $a:b$ phase synchrony (Tass et al., 1998). They can be quantified with different measures, like the PSI, the envelope-to-signal correlation (Bruns and Eckhorn, 2004) or the modulation index (Canolty et al., 2006). The adaptive methods presented in this paper are especially relevant in such cases. Indeed, these coupling measures could take advantage of signals where the oscillations are precisely extracted.

In conclusion, this novel adaptive scheme can be used as an additional processing step for the analysis of EEG data. It is particularly attractive when precise oscillation extraction is required or when coupling measures based on phase are applied (like the PSI).

Acknowledgments

We thank the anonymous reviewers for helpful and constructive comments. This work was supported by Swiss National Science Foundation grant 320030-120579. The Cartool soft-

ware (<http://brainmapping.unige.ch/Cartool.htm>) has been programmed by Denis Brunet, from the Functional Brain Mapping Laboratory, Geneva, Switzerland, and is supported by the Center for Biomedical Imaging (CIBM) of Geneva and Lausanne.

References

- Bruns A, Eckhorn R. Task-related coupling from high- to low-frequency signals among visual cortical areas in human subdural recordings. *Int J Psychophysiol* 2004;51:97–116.
- Buzsaki G. *Rhythms of the brain*. first ed New York: Oxford University Press; 2006.
- Canolty RT, Edwards E, Dalal SS, Soltani M, Nagarajan SS, Kirsch HE, et al. High-gamma power is phase locked to theta oscillations in human neocortex. *Science* 2006;313:1626–8.
- Celka P. Statistical analysis of the phase-locking value. *IEEE Signal Process Lett* 2007;14(9):577–80.
- Chavez M, Besserve M, Adam C, Martinerie J. Towards a proper estimation of phase synchronization from time series. *J Neurosci Meth* 2006;154:149–60.
- Demiralp T, Bayraktaroglu Z, Lenz D, Junge S, Busch NA, Maess B, et al. Gamma amplitudes are coupled to theta phase in human EEG during visual perception. *Int J Psychophysiol* 2007;64(1):24–30.
- Engel AK, Fries P, Singer W. Dynamic predictions: oscillations and synchrony in top-down processing. *Nature* 2001;2(10):704–16.
- Engel AK, Singer W. Temporal binding and the neural correlates of sensory awareness. *Trends Cogn Sci* 2001;5:16–25.
- Flandrin P. Time–frequency/time-scale analysis. San Diego: Academic Press; 1999.
- Freeman WJ, Rogers LJ, Holmes MD, Silbergeld DL. Spatial spectral analysis of human electrocorticograms including the alpha and gamma band. *J Neurosci Meth* 2000;95:111–21.
- Fries P. A mechanism for cognitive dynamics: neuronal communication through neuronal coherence. *Trends Cogn Sci* 2005;9:474–80.
- Gabor D. Theory of communication. *J IEE Lond* 1946;93:429–57.
- Gonzalez Andino SL, Michel CM, Thut G, Landis T, Grave de Peralta R. Prediction of response speed by anticipatory high-frequency (gamma band) oscillations in the human brain. *Hum Brain Mapp* 2005a;24(1):50–8.
- Gonzalez Andino SL, Murray MM, Foxe JJ, Grave de Peralta Menendez R. How single-trial electrical neuroimaging contributes to multisensory research. *Exp Brain Res* 2005b;166(3–4):298–304.
- Haykin S. *Adaptive filter theory*. fourth ed New Jersey: Prentice Hall; 2001.
- Jacobs J, Kahana MJ, Ekstrom AD, Fried I. Brain oscillations control timing of single-neuron activity in humans. *J Neurosci* 2007;27(14):3839–44.
- Jarque CM, Bera AK. A test for normality of observations and regression residuals. *Int Stat Rev* 1987;55(2):163–72.
- Jensen O, Colgin LL. Cross-frequency coupling between neuronal oscillations. *Trends Cogn Sci* 2007;11(7):267–9.
- Lachaux J, Rodriguez E, Martinerie J, Varela F. Measuring phase synchrony in brain signal. *Hum Brain Mapp* 1999;8:194–208.
- Lakatos P, Chen CM, O'Connell MN, Mills A, Schroeder CE. Neuronal oscillations and multisensory interaction in primary auditory cortex. *Neuron* 2007;53(2):279–92.
- Liao H. Two discrete oscillator based adaptive notch filters (OSC ANFs) for noisy sinusoids. *IEEE Trans Signal Process* 2005;53(2):528–38.
- Linkenkaer-Hansen K, Nikulin VV, Palva S, Ilmoniemi RJ, Palva JM. Prestimulus oscillations enhance psychophysical performance in humans. *J Neurosci* 2004;24(45):10186–90.
- Martuzzi R, Murray MM, Meuli RA, Thiran JP, Maeder PP, Michel CM, et al. Methods for determining frequency- and region-dependent relationships between estimated LFPs and BOLD responses in humans. *J Neurophysiol* 2009;101(1):491–502.
- Mormann F, Lehnertz K, David P, Elger CE. Mean phase coherence as a measure for phase synchronization and its application to the EEG of epilepsy patients. *Physica D* 2000;144:358–69.
- Murray MM, Wyllie GR, Higgins BA, Javitt DC, Schroeder CE, Foxe JJ. The spatiotemporal dynamics of illusory contour processing: combined high-density electrical mapping, source analysis, and functional magnetic resonance imaging. *J Neurosci* 2002;22(12):5055–73.
- Nho W, Loughlin PJ. When is instantaneous frequency the average frequency at each time? *IEEE Signal Process Lett* 1999;6(4):78–80.
- Penny WD, Duzel E, Miller KJ, Ojemann JG. Testing for nested oscillation. *J Neurosci Meth* 2008;174:50–61.
- Prudat Y, Vesin JM. Multi-signal extension of adaptive frequency tracking algorithms. *Signal Process* 2009;89(6):963–73.
- Quiñero Quiroga R, Kraskov A, Kreuz T, Grassberger P. Performance of different synchronization measures in real data: a case study on electroencephalographic signals. *Phys Rev E* 2002;65:041903.
- Rao A, Kumaresan R. On decomposing speech into modulated components. *IEEE Trans Speech Audio Process* 2000;8(3):240–54.
- Schroeder CE, Lakatos P. Low-frequency neuronal oscillations as instruments of sensory selection. *Trends Neurosci* 2009a;32(1):9–18.
- Schroeder CE, Lakatos P. The gamma oscillation: master or slave? *Brain Topogr* 2009b;22(1):24–6.
- Singer W, Gray CM. Visual feature integration and the temporal correlation hypothesis. *Annu Rev Neurosci* 1995;18:555–86.
- Tass P, Rosenblum MG, Weule J, Kurths J, Pikovsky A, Volkmann J, et al. Detection of n:m phase locking from noisy data: application to magnetoencephalography. *Phys Rev Lett* 1998;81(15):3291–4.
- Tallon-Baudry C, Bertrand O. Oscillatory gamma activity in humans and its role in object representation. *Trends Cogn Sci* 1999;3(4):151–62.
- Uldry L, Duchêne C, Prudat Y, Murray MM, Vesin JM. Adaptive tracking of EEG frequency components. In: Naït-Ali A, editor. *Advanced biosignal processing*. New York: Springer; 2009.
- Varela FJ, Thompson E, Rosch E. *The embodied mind*. Cambridge: MIT Press; 1991.
- Varela F, Lachaux JP, Rodriguez E, Martinerie J. The brainweb: phase synchronization and large-scale integration. *Nat Rev Neurosci* 2001;2:229–39.
- Von Stein A, Sarnthein J. Different frequencies for different scales of cortical integration: from local gamma to long range alpha/theta synchronization. *Int J Psychophysiol* 2000;38:301–13.
- Womelsdorf T, Fries P, Mitra PP, Desimone R. Gamma-band synchronization in visual cortex predicts speed of change detection. *Nature* 2006;439(7077):733–6.